PASJ: Publ. Astron. Soc. Japan , 1–??,

Hinode EUV Imaging Spectrometer Observations of Solar Active Region Dynamics

John T. Mariska,[1] Harry P. Warren,[1] Ignacio Ugarte-Urra,[2] David H. Brooks,[2] David R. Williams,[3] and Hirohisa Hara[4]

[1]*Space Science Division, Naval Research Laboratory, Washington DC 20375, USA*
mariska@nrl.navy.mil

[2]*George Mason University, 4400 University Drive, Fairfax, VA 22020, USA*

[3]*Mullard Space Science Laboratory, University College London, Holmbury St. Mary, Dorking, Surrey, RH5 6NT, UK*

[4]*National Astronomical Observatory, Mitaka, Tokyo 181-8588*

(Received 2007 June 5; accepted 2007 August 29)

Abstract

The EUV Imaging Spectrometer (EIS) on the Hinode satellite is capable of measuring emission line center positions for Gaussian line profiles to a fraction of a spectral pixel, resulting in relative solar Doppler-shift measurements with an accuracy of less than a km s^{-1} for strong lines. We show an example of the application of that capability to an active region sit-and-stare observation in which the EIS slit is placed at one location on the Sun and many exposures are taken while the spacecraft tracking keeps the same solar location within the slit. For the active region examined (NOAA 10930), we find that significant intensity and Doppler-shift fluctuations as a function of time are present at a number of locations. These fluctuations appear to be similar to those observed in high-temperature emission lines with other space-borne spectroscopic instruments. With its increased sensitivity over earlier spectrometers and its ability to image many emission lines simultaneously, EIS should provide significant new constraints on Doppler-shift oscillations in the corona.

Key words: Sun: corona — Sun: oscillations — Sun: UV radiation

1. Introduction

The EUV Imaging Spectrometer (EIS) on Hinode uses multilayer optics to produce stigmatic spectra in two 40 Å wide EUV bands centered at 195 and 270 Å. Emission lines present in these bands originate in the solar transition region and corona, permitting detailed study of the temperature, density, and dynamical structure of these regions. The Hinode mission is described in Kosugi et al. (2007). An overall description of EIS is available in Culhane et al. (2007). Lang et al. (2006) provides more detailed information on the EIS calibration, and Korendyke et al. (2006) provides details of the optics and mechanisms.

EIS can image the Sun using 1″ and 2″ slits and 40″ and 266″ slots. The latter result in monochromatic images of the Sun in the stronger spectral lines. Obtaining the full diagnostic capability of the instrument, however, is only possible when data are acquired with the 1″ or 2″ slits. This means that images must be constructed by moving the EIS mirror to raster an area of interest. There is, of course, a scientific tradeoff to be made for constructing a spectroheliogram in this manner—it can take considerable time. For an exposure time of 30 s, a typical value for capturing both the strongly- and weakly-emitting portions of an active region, it can take an hour or more to image a substantial area of the disk.

When high time cadence is important, a better approach is to use EIS in a sit-and-stare mode. In this case, the 1″ or 2″ slit is placed at one location on the Sun and repeated exposures are obtained while the Hinode spacecraft tracks the solar rotation so that the slit always samples the same solar plasma. These kinds of observations can be enhanced by preceding and/or following them with EIS spectroheliograms, and are, of course, further enhanced by using imaging data from the Hinode X-Ray Telescope (XRT) to monitor the overall evolution of the area being examined with the sit-and-stare observation. Details of the capabilities of the XRT on Hinode are available in Golub et al. (2007).

In this paper, we present some initial results from one EIS sit-and-stare data set. The focus here is on small fluctuations in an active region. Imada et al. (2007) discuss additional EIS dynamical observations during the gradual phase of an X-class flare.

2. Observations

The observations discussed in this contribution cover portions of NOAA active region 10930 and were obtained on 2006 December 14, when it was located at approximately S05W39. EIS spectroheliograms covering portions of the active region were obtained beginning at 3:23 and 19:20 UT. Each spectroheliogram consisted of 256 30 s exposures with the 1″ slit and a spatial step size between exposures of 1″, taking approximately 2 hr 23 m to complete. A 120-exposure EIS sit-and-stare observation within the

Table 1. Emission lines observed with EIS

Ion	Wavelength (Å)	Log $T_{\max}$ (K)
Fe VIII	185.21	5.56
Fe X	184.54	5.98
Fe XII	195.12	6.11
Fe XIII	202.04	6.20
Fe XIV	274.20	6.28
Fe XV	284.16	6.32

region was begun at 17:00 UT. That study used 60 s exposures.

For both the spectroheliograms and the sit-and-stare observations, nine data windows were selected on the EIS detectors. This paper only presents results for the lines in six of those windows. Each window in the spectroheliograms was 24 spectral pixels wide and covered a 256″ region of the Sun in the N/S direction. For the sit-and-stare data set, each window was 32 spectral pixels wide, but the slit covered a 512″ region in the N/S direction. Each EIS spectral pixel is 22.3 mÅ wide. The measured FWHM at 185 Å is 47 mÅ (Culhane et al. 2007). Table 1 lists the emission lines included in this study and their temperatures of formation.

Figure 1 shows an XRT image of the active region taken at 19:19:52 UT with a box marking the region covered by the EIS spectroheliogram that followed the sit-and-stare observation and a vertical line showing the position of the EIS slit during the sit-and-stare observation. The image was obtained with the XRT Be_thin/Open filter combination, which has peak sensitivity at a temperature of roughly 10 MK and is two orders of magnitude less sensitive at about 2 MK (Golub et al. 2007). Thus, the image is mostly dominated by emission at higher temperatures than those seen in most of the EIS emission lines used in this study.

All the data were processed using the current version of the EIS data preparation software. This removed the detector bias and dark current, as well as hot pixels and cosmic ray hits, and then applied the EIS absolute calibration, yielding intensities in ergs cm^{-2} s^{-1} sr^{-1} Å^{-1}. The software replaces the hot pixels and those affected by cosmic ray hits with interpolated values from adjoining pixels, but the data at those locations were flagged as bad and the line fitting software gave those locations no weight in the subsequent line profile fitting process. The data on the long-wavelength detector were also shifted in the y-direction to account for the roughly 17 pixel offset between the two detectors.

Figure 2 shows the appearance of the active region in the EIS spectroheliograms taken immediately after the sit-and-stare study. The vertical line on each panel shows the location of the EIS slit during the sit-and-stare observation. As the images show, the portions of the active region imaged by EIS had a complex structure. Examination of movies made from XRT images of the active region shows that considerable flare-like activity was taking place throughout the time of the EIS observations. Data from the GOES X-ray monitors also show significant flare-like fluctuations at the B to C level, and an X-flare took place later in the day. The bright, compact loops in the XRT image are the result of a small flare that took place before the EIS slit reached those positions. By the time the EIS slit reached those positions, the strong emission had decayed and the loop morphology is less evident. (EIS spectroheliograms are constructed by scanning the slit from west to east on the Sun.)

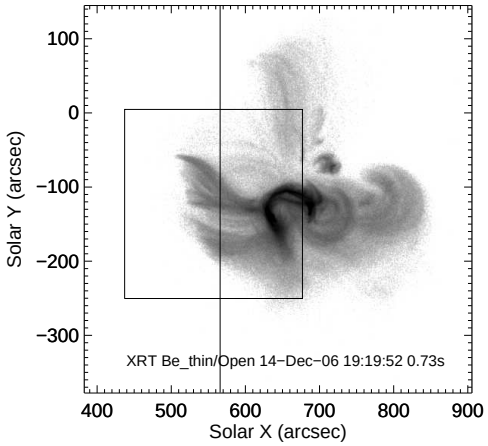

Fig. 1. An XRT image of NOAA active region 10930 showing the location of the EIS spectroheliogram taken from 19:20:12 to 21:34:55 UT, and the slit location for the EIS sit-and-stare observation taken from 17:00:20 to 19:04:06 UT. The coordinate system on the figure corresponds to the time of the XRT exposure and the EIS spectroheliogram and slit location have been rotated to that time.

3. Intensity and Doppler-shift fluctuations

For the sit-and-stare observation, the emission lines in the six wavelength bands shown in Figure 2 were all fitted with single Gaussian line profiles. Thus, for each spectral line at each location along the EIS slit, we have measured values of the total line intensity, the location of the line center, and the line width. Figure 3 shows a greyscale representation of the resulting total intensity in each spectral line as a function of time for all 512 positions along the slit. A number of locations show obvious evidence for rapid time variations in the total intensity. Comparison with the EIS spectroheliograms in Figure 2 shows that these locations appear to correspond generally to areas near the footpoints of loops. Examination of movies made from the XRT images and those from the EUV Imaging Telescope (EIT) on the Solar and Heliospheric Observatory (SOHO) suggest that these are due to intermittent heating events in some of the loops crossed by the EIS slit.

Extracting Doppler-shift information is a somewhat complex undertaking. The EIS slit is not perfectly vertical on the camera CCDs, so a correction for the slit tilt must be made. In addition, over the course of each orbit, EIS

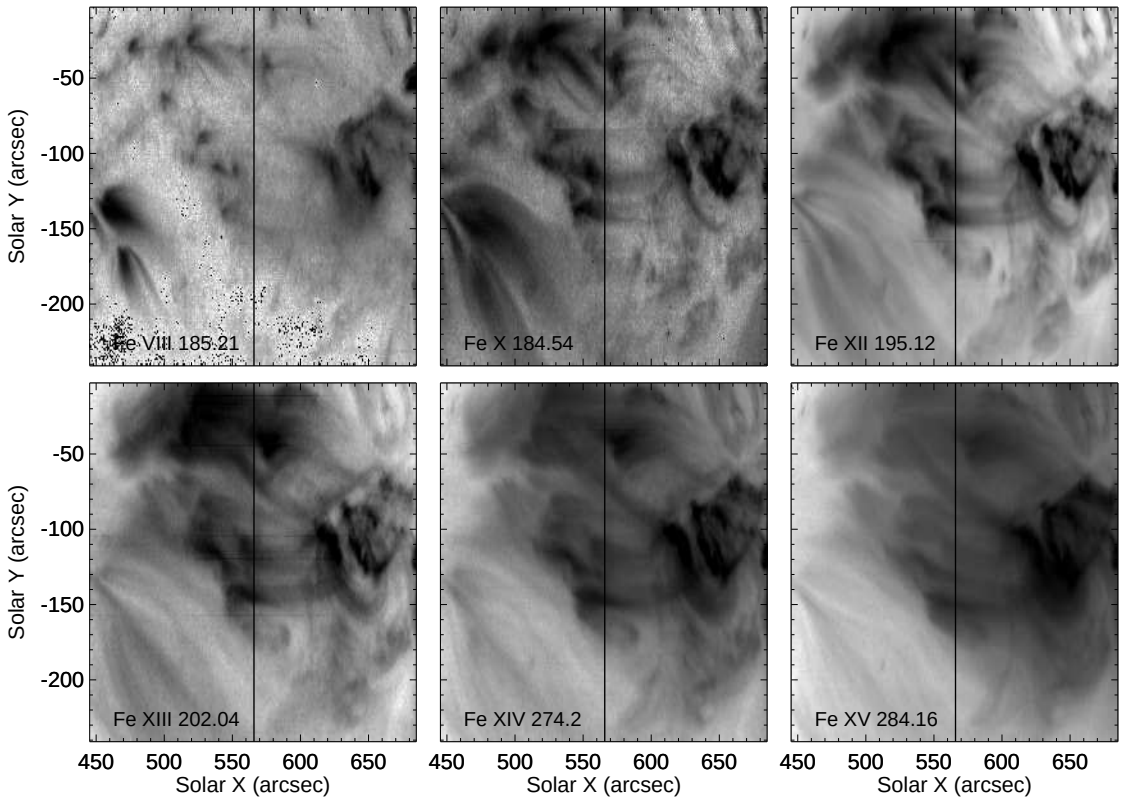

Fig. 2. EIS spectroheliograms in six different emission lines obtained from 19:20:12 to 21:34:55 UT on 2006 December 14. The vertical line in each plot shows the position of the EIS 1″ slit during the sit-and-stare observation, which was taken from 17:00:20 to 19:04:06 UT. The coordinate system for the figure corresponds to the time of the middle of the spectroheliogram.

exhibits a periodic variation in the measured line center position for all spectral lines observed in both detectors. The peak-to-peak variation is about 2 spectral pixels—a significant Doppler signal at the wavelengths covered by EIS. The cause of this variation is still under investigation, but appears to be due to temperature changes within the instrument.

The slit tilt does not appear to change with time and results in a difference in the location of the rest wavelength for an emission line of approximately 0.37 spectral pixels from the bottom to the top of the 512″ slit length used in the sit-and-stare observations. While this is small, it represents a velocity change of about 13 km s^{-1} at the Fe XII 195.12 Å emission line and thus is important for detailed dynamical studies. The slit tilt was removed from the sit-and-stare data set by shifting the fitted line center position in each spectral line by an amount determined using an analysis of Doppler-shift data taken early in the mission.

To a first approximation, the orbital variation is the same at each location on the two EIS detectors. Thus, it is possible to use the data in a high-signal-to-noise channel during the sit-and-stare observation to determine the orbital variations for all the wavelengths. To do this we use the top 112 rows of fitted line center positions (corrected for slit tilt) in the Fe XII 195.12 Å emission line data to determine an average orbital variation. This orbital variation is then subtracted from the line center positions measured in all the wavelength windows. This particular region was selected because examination of the XRT and EIT data indicates that no significant dynamical activity is present at these locations. Note that EIS has no absolute wavelength reference. Once the orbital trend has been removed using the Fe XII 195.12 Å emission line data, the average value of the line center position in the top 112 rows in each of the six emission lines used in this study was used as the rest wavelength for that emission line.

Figure 4 shows a greyscale representation of the fitted line center positions with the orbital variations removed as a function of time for all 512 positions along the slit for the six lines included in this study. In these images darker shades represent smaller values for the Doppler shift (blueshifts). If one excludes data points that are obvious outliers because of poor Gaussian fits, the range of Doppler-shift velocities seen in the panels is on the order of 20 to 100 km s^{-1}.

Examination of the sit-and-stare images shown in Figures 3 and 4 shows that all the significant features shown along the slit location in the the spectroheliograms shown in Figure 2 are present in the sit-and-stare data.

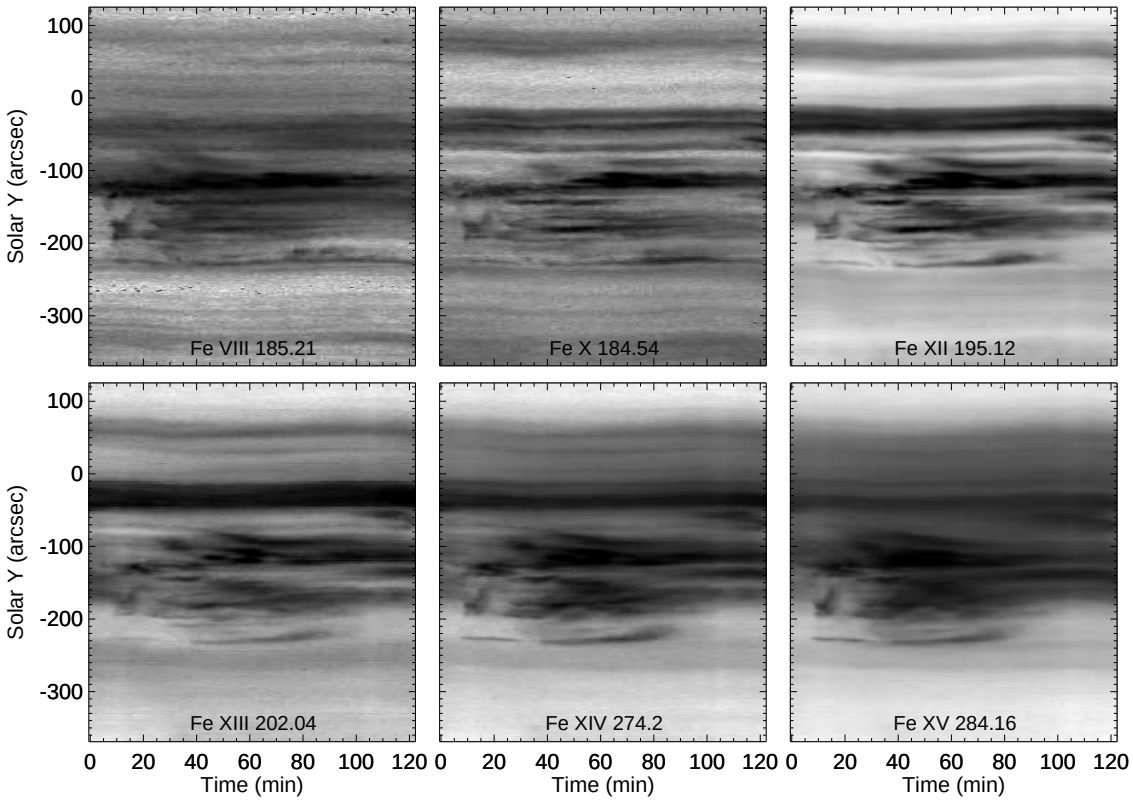

Fig. 3. EIS sit-and-stare intensity data in six different emission lines obtained beginning at 17:00:20 UT on 2006 December 14. The horizontal axis values are the start times of the exposures.

Near the top of this Y-range (roughly $-10''$ to $-40''$, there are nearly constant intensity bands in all the emission lines. Examination of the spectroheliograms and especially of a movie made from the EIT 195 Å images shows that these are quiescent loops interconnecting portions of the active region. The Doppler-shift sit-and-stare data at these locations show little or no time-dependent fluctuation in any of the emission lines observed with EIS.

In contrast, the Y-range from $-100''$ to $-230''$ shows considerable time-dependent behavior in both the line intensity and the Doppler shift. While the intensity variations are visible in all the emission lines, there is a clear tendency for the Doppler shifts to become more pronounced as the temperature of formation of the emission line increases.

Figure 5 shows greyscale images of the Fe XII and Fe XV intensity and Doppler-shift data along the portion of slit where considerable activity is taking place. Some features are clearly impulsive, such as the upflow at $-180''$ and 10 min and a second at $-160''$ and 15 min seen in the Fe XII and Fe XV lines. More gradual changes in the Doppler shifts are also evident. For example, in both the Fe XII and Fe XV Doppler images in the vicinity of -160 and 60 min, the redshift velocities appear to be changing gradually over 20-min and longer timescales.

Figure 6 shows intensity and Doppler-shift data in the Fe XII and Fe XV emission lines as a function of time at a solar Y-position of approximately $-185''$. The graphs quantify the impression given in Figure 5—an impulsive event of some kind has taken place causing a relative blueshift followed by a relative redshift. In the Doppler-shift plots and to a lesser degree in the intensity plots, the events appear to be superimposed on a more smoothly varying background.

The Doppler shifts in both the Fe XII and Fe XV emission lines appear to show roughly one complete oscillation. In the intensity plots, the full oscillation is less obvious, possibly because the signal is superimposed on the more gradual trend present in the data. Measuring the time between the maximum blueshift and the maximum redshift in each line and assuming that it corresponds 1/2 the oscillation period, results in oscillation periods of 8.2 min for the Fe XII emission line and 10.2 min for the Fe XV emission line. Given the one-minute cadence of the sit-and-stare observation, these numbers should be considered roughly equal.

Measuring the time between the intensity peak and the following local minimum and assuming that it corresponds to 1/2 the oscillation period results in oscillation periods of 14.4 and 16.4 min for the Fe XII and Fe XV emission lines, respectively. Thus, the intensity fluctuations do not have the same period as the Doppler-shift fluctuations.

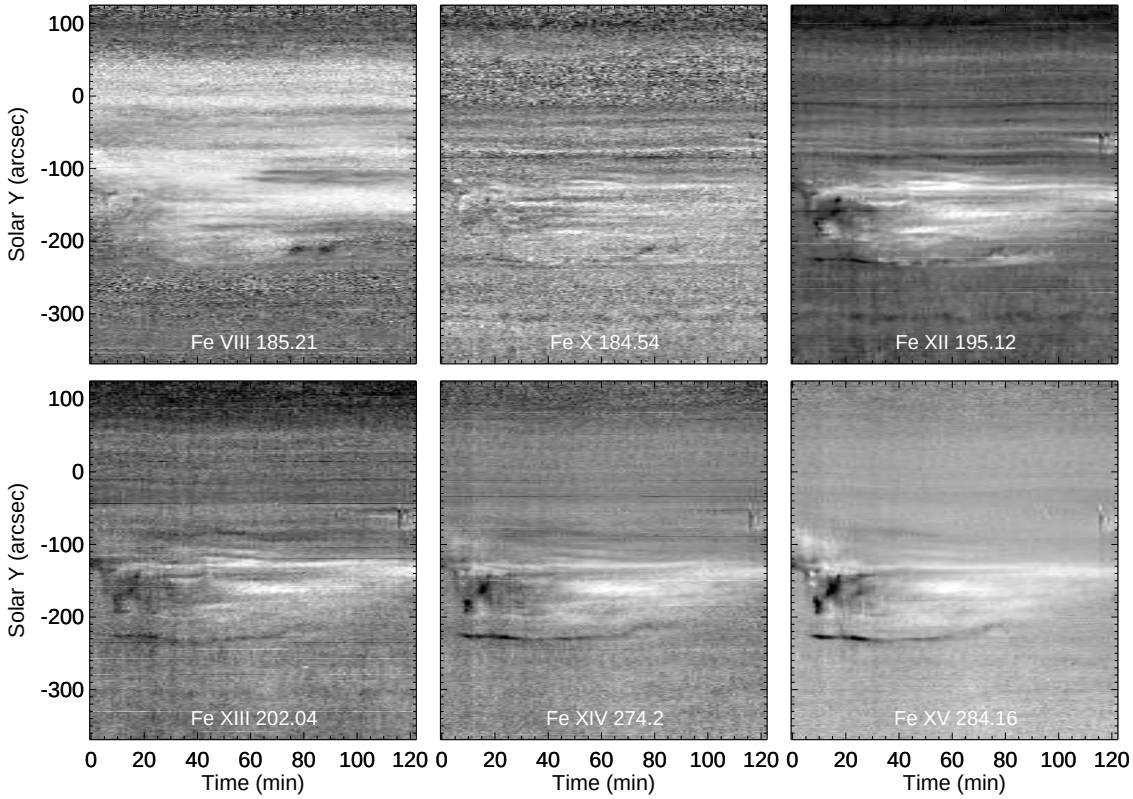

Fig. 4. EIS sit-and-stare Doppler-shift data in six different emission lines obtained beginning at 17:00:20 UT on 2006 December 14. The horizontal axis values are the start times of the exposures. Darker values represent smaller numbers (blueshifts). The zero point for the Doppler shifts is arbitrary. The range of Doppler shifts is 374 km s^{-1} for Fe VIII, 88 km s^{-1} for Fe X, 28 km s^{-1} for Fe XII, 25 km s^{-1} for Fe XIII, 42 km s^{-1} for Fe XIV, and 266 km s^{-1} for Fe XV.

Note also that the peak in the intensity oscillation appears to be later than the maximum blueshift.

The characteristics of the intensity and Doppler-shift oscillations show in Figure 6 are very similar to those observed for example by Wang et al. (2003) and Wang et al. (2005) using the SUMER spectrometer on SOHO. Wang et al. (2005) reported average oscillation periods of 17.9 ± 5.5 min with a range from 8.6 to 23.3 min, comparable to the oscillation shown in the figure. They reported a wide range of Doppler shift amplitudes—ranging from 12 to 353 km s^{-1}, with an average value of 62 ± 57 km s^{-1}. We find amplitudes of roughly 6.5 and 25.8 km s^{-1} for the Fe XII and Fe XV emission lines, respectively, within the range seen in the SUMER observations.

Note that for the most part the Doppler shift velocities are quite small, and one might ask whether EIS is capable of measuring such small velocity changes. Figure 7 shows sample Fe XII and Fe XV spectral data taken near the peak in the Doppler-shift plots along with the best-fit Gaussians. The one-σ uncertainties on the fits are 0.44 and 0.63 km s^{-1} for the Fe XII and Fe XV data, respectively. This level of accuracy is achievable with EIS whenever the signal level is high and a Gaussian represents a good functional form for the line profile.

4. Conclusions

The sit-and-stare observations presented in this paper and other similar EIS active region observations clearly show an abundance of dynamical phenomena in active regions, much of it periodic. Cotemporal XRT imaging data often show that these phenomena are the dynamical manifestation of disturbances that can be seen following field lines that interconnect portions of the active region. Thus, careful analysis of combined EIS and XRT data sets should provide an improved picture of how active regions evolve. Ultimately, the addition of chromospheric images and vector magnetograms from the Solar Optical Telescope on Hinode should make it possible to begin to connect fully changes in the corona with the evolution of the underlying magnetic field.

The particular example shown in Figure 6 is similar to oscillatory phenomena observed in high-temperature emission lines with the SUMER spectrometer on SOHO. The intensity signal shown near $-185''$ in Figure 5 does begin with a fairly low intensity, and one might speculate that higher temperature plasma in emitting at that time at that location. The data set we have analyzed for this study does not include the hotter line of Fe XVII at

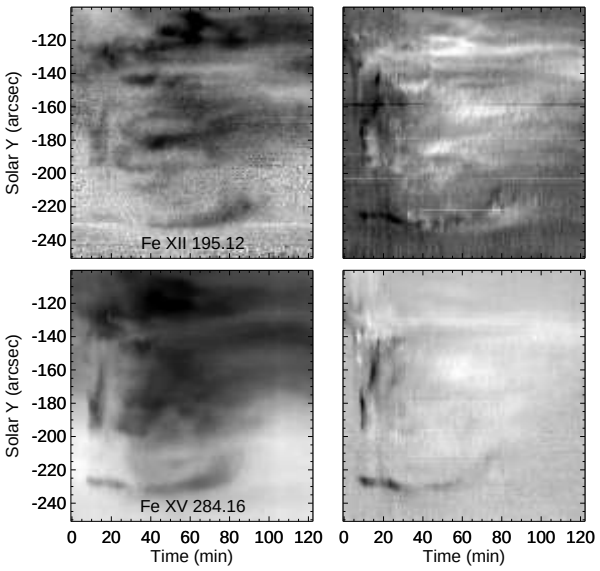

Fig. 5. EIS sit-and-stare intensity (left panels) and Doppler-shift (right panels) data for Fe XII and Fe XV for a portion of slit range covered by Figures 3 and 4. For the Doppler shift data, darker values represent smaller numbers (blueshifts). The zero point for the Doppler shifts is arbitrary. The range of Doppler shifts is 87 km s^{-1} for Fe XII and 96 km s^{-1} for Fe XV.

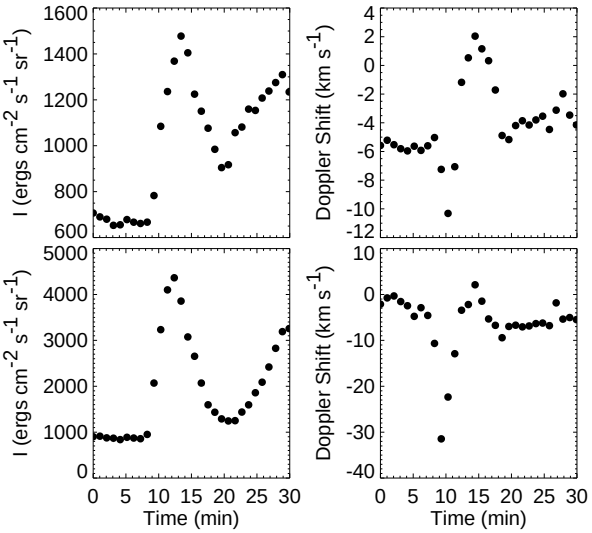

Fig. 6. EIS sit-and-stare intensity and Doppler-shift data for Fe XII (top row) and Fe XV (bottom row) for a solar Y-position near $-185''$. Negative values for the Doppler shift represent blueshifted emission. The zero-velocity point has been arbitrarily set to the average value for all 120 measurements at this Y-position.

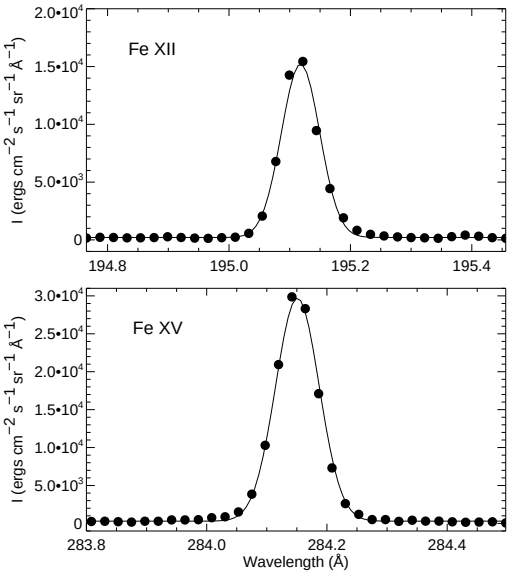

Fig. 7. Sample Fe XII 195 Å and Fe XV 284 Å spectral window data obtained at a solar Y-position of $-185''$ at 17:14:48 UT, near the peak in the Doppler shift plots shown in Figure 6. The lines show the best fit Gaussian to each data set.

204.65 Å available in the EIS bandpass, and, while we do have data for the Ca XVII emission line at 192.82 Å, the line suffers from a blend with a cooler line of Fe XI, which can only be removed with information from other Fe XI lines. Thus, a full comparison with SUMER results must await the analysis of additional data.

Many of these events are thought to be standing slow-mode waves, the detailed study of which should lead to a better understanding of heating in coronal loops. Because EIS is a more sensitive instrument than SUMER, shorter exposure times are possible, which should allow us to expand the range of periods that can be investigated. Moreover, the EIS wavelength bands contain lines whose ratios are sensitive to coronal electron densities, leading to better constraints on the characteristics of the oscillations.

Extracting subtle dynamical information from EIS data does, however, require both carefully planned observations and an analysis that pays attention to all the possible instrumental effects. Many of the instrumental effects are just beginning to be understood, so it may be some time before it is possible to fully realize the potential EIS offers for more completely characterizing solar coronal dynamics.

Hinode is a Japanese mission developed and launched by ISAS/JAXA, with NAOJ as domestic partner and NASA and STFC (UK) as international partners. It is operated by these agencies in cooperation with ESA and NSC (Norway). We are grateful to the entire Hinode team for all their efforts in the design and operation of the mission. JTM, HPW, IUU, and DHB acknowledge support from the NASA Hinode program.

References

Culhane, J. L., et al. 2007, Sol. Phys., in press
Golub, L., et al. 2007, Sol. Phys., in press
Imada, S., et al. 2007, PASJ, in press
Korendyke, C. M., et al. 2006, Appl. Opt., 45, 8674
Kosugi, T., et al. 2007, Sol. Phys., to be submitted
Lang, J., et al. 2006, Appl. Opt., 45, 8689
Wang, T. J., Solanki, S. K., Curdt, W., Innes, D. E., Dammasch, I. E., & Kliem, B. 2003, A&A, 406, 1105
Wang, T. J., Solanki, S. K., Innes, D. E., & Curdt, W. 2005, A&A, 435, 753